Food Chemistry 270 (2019) 1–9

Contents lists available at ScienceDirect

Food Chemistry

journal homepage: www.elsevier.com/locate/foodchem

Patulin removal from apple juice using a novel cysteine-functionalized metal-organic framework adsorbent

Manshun Liu[a], Jing Wang[a], Qingfeng Yang[a], Na Hu[b], Wentao Zhang[a], Wenxin Zhu[a], Rong Wang[a], Yourui Suo[b], Jianlong Wang[a,*]

[a] College of Food Science and Engineering, Northwest A&F University, Yangling 712100, Shaanxi, China
[b] Qinghai Key Laboratory of Qinghai-Tibet Plateau Biological Resources, Northwest Institute of Plateau Biology, Chinese Academy of Sciences, Qinghai 810008, China

ARTICLE INFO

Chemical compounds studied in this article:
Zirconium chloride (PubChem CID: 24817)
2-Amino terephthalic acid (PubChem CID: 2724822)
Sodium borohydride (PubChem CID: 23673181)
N,N′-dimethylformamide (PubChem CID: 6228)
Patulin (PubChem CID: 4696)
Chloroauric acid (PubChem CID: 28133)
Acetonitrile (PubChem CID: 6342)
Gallic acid (PubChem CID: 370)
Folin-Ciocalteu reagent (PubChem CID: 6342)
2,6-Dichloroindophenol sodium salt (PubChem CID: 23697355)
Vitamin C (PubChem CID: 54670067)
Thiazol tetrazolium bromide (PubChem CID: 64965)
Dimethylsulfoxide (PubChem CID: 579)

Keywords:
Metal-organic framework
Adsorbent
Patulin removal
Time-saving

ABSTRACT

Patulin (PAT) is one of the most common toxic contaminants of apple juice, which causes severe food safety issues throughout the apple industry. In order to remove PAT efficiently, a metal-organic framework-based adsorbent (UiO-66(NH_2)@Au-Cys) was successfully synthesized and used for PAT removal from juice-pH simulation solution and real apple juice. Batch adsorption experiments were systematically performed to study the adsorption behavior for PAT. The results showed that adsorption process could be well described by the Pseudo-second order model and Freundlich isotherm model. The maximum adsorption capacity (4.38 μg/mg) was 10 times higher than the microbe-based biosorbents. Thermodynamic investigation demonstrated that adsorption process was spontaneous and endothermic. Furthermore, no marked cytotoxicity on NIH 3T3 cell lines was observed when the concentration of the adsorbent was lower than 10 μg/mL. Therefore, UiO-66(NH_2)@Au-Cys is a potential adsorbent for PAT removal from apple juice with little quality changes.

1. Introduction

Patulin (PAT, $C_7H_6O_4$) is a type of water soluble mycotoxin that has been frequently found in numerous fruits and vegetables. Apples are susceptible to be infected by fungus and always serve as a suitable medium for PAT production during the harvest, storage and even processing. Moreover, PAT also existed in apple derivative products ranging from non-fermented apple juice to apple purees, which was ascribed to the wake effect of the most types of food processing on the overall stability of PAT (Beltrán, Ibáñez, Sancho, & Hernández, 2014; Sanzani, Reverberi, Punelli, Ippolito, & Fanelli, 2012; Tannous et al., 2017). Due to the detrimental effects on humans, such as edema, diarrhea and intestinal inflammation (Boussabbeh et al., 2015; Puel, Galtier, & Oswald, 2010), the concentration of PAT was considered as a crucial quality standard of apple juice productions, for which the majority of regulatory agencies had placed caps on PAT concentration at the level of 50 μg/kg in apple juice (U.S. Food and Drug Administration, 2013). Additionally, with the remarkable increasing of the apple juice consumption throughout the world, PAT contamination in apple juice not only caused widespread worries about food safety but also resulted in enormous financial losses (Peng et al., 2016). Therefore, it is necessary to remove PAT from apple juice to meet the increasingly

* Corresponding author.
E-mail address: wanglong79@nwsuaf.edu.cn (J. Wang).

https://doi.org/10.1016/j.foodchem.2018.07.072
Received 31 March 2018; Received in revised form 11 July 2018; Accepted 11 July 2018
Available online 14 July 2018
0308-8146/

stringent food quality standards and food safety requirements.

There were various physical and chemical approaches developed to solve the problem of PAT contamination in apple juice, such as radio-degradation, sulfur dioxide treatment and oxidation with ammonia or potassium permanganate (Moake, Padilla-Zakour, & Worobo, 2005; Yun et al., 2008). Among the reported methods, adsorption was considered as one of the most effective processes to remove PAT (Qiu, et al., 2018). On this account, developing an efficient and reliable adsorbent has been considered as an active demand. To date, various adsorbents, such as activated carbon, alginate gel (Yue et al., 2013), cyclodetrin-based polymer (Appell & Jackson, 2010), propylthiol functionalized SBA-15 silica (Appell, Jackson, & Dombrink-Kurtzman, 2011), chitosan-based materials (Li, Wang, Meng, & Liu, 2015; Liu et al., 2015; Luo, Zhou, & Yue, 2017; Peng et al., 2016) and some microorganisms including yeast and lactic acid bacteria (Luo, Wang, Yuan, Zhou, & Yue, 2016; Wang et al., 2015), had been reported to considerably decrease PAT levels in contaminated apple juice and other liquids. However, these adsorbents did not satisfy the requirements for apple juice industry since their negative effects on juice quality such as clarity, brix and pH. Moreover, a tedious and complex adsorption process was needed for the application of the reported adsorbents, such as multi-step preparation of adsorbent and requirement of long adsorption time (at least 10 h). Therefore, it is urgent to exploit a new adsorbent with enhanced absorption capacity and high efficiency for PAT removal without deteriorating the quality of the products.

Metal-organic frameworks (MOFs) as a kind of novel adsorbent had attracted tremendous research interests because of their fascinating properties, such as high internal surface area and wide turnable composition (Wang et al., 2017; Yang, Wang, Chen et al., 2018). Zirconium-based MOFs gained additional attention due to the stability toward moisture and acids (Cavka et al., 2008; Peterson, Mahle, DeCoste, Gordon, & Rossin, 2016; Yang, Wang, Wang et al., 2018). Given the attractive features of the zirconium-based MOF materials, UiO-66(NH_2) was chosen as the adsorbent for PAT removal. However, the lack of binding sites for the target toxin was the great obstacle for the utilization of UiO-66(NH_2). Thus we hypothesized that the chemical modification for UiO-66(NH_2) could improve the adsorption efficiency for PAT removal.

In this work, a cysteine-functionalized UiO-66(NH_2)-based adsorbent (UiO-66(NH_2)@Au-Cys) was successfully synthesized and used to efficiently remove PAT from apple juice via its abundant active sites including amine, hydroxyl and carboxyl that were obtained from Cys. Parameters (such as pH, temperature and adsorption time) influencing the adsorption capacity of UiO-66(NH_2)@Au-Cys were optimized. Moreover, kinetic, isotherm and thermodynamic study were also performed to illustrate the characteristics of UiO-66(NH_2)@Au-Cys during the PAT adsorption process. Furthermore, the cytotoxicity and PAT removal capacity of the proposed adsorbent in apple juice were also evaluated. Variation of brix, titratable acidity, clarity, total phenol and vitamin C content were measured to evaluate the influence of UiO-66(NH_2)@Au-Cys on the quality of apple juice during PAT adsorption process.

2. Materials and methods

2.1. Chemicals

Zirconium chloride ($ZrCl_4$), 2-amino terephthalic acid (H_2BDC-NH_2), sodium borohydride ($NaBH_4$), N,N′-dimethylformamide (DMF), standard patulin, vitamin C powder, 2,6-dichloroindophenol sodium salt, methyl thiazol tetrazolium bromide (MTT) and dimethylsulfoxide (DMSO) were purchased from Aladdin Chemical Reagent Co., Ltd, China. In addition, Dulbecco's Modified Eagle Medium (DMEM) and chloroauric acid ($HAuCl_4{\cdot}3H_2O$) were purchased from Sigma-Aldrich. All other chemicals used in the experiment were obtained from the local chemical reagent company. All of the above chemicals were at least analytical grade. The mobile phase (acetonitrile) of chromatographic analysis was HPLC-grade. Ultrapure water produced by Milli-Q element (18.2 X, Millipore, Massachusetts) was used to prepare all of the solutions.

2.2. Synthesis of UiO-66(NH_2)@Au-Cys adsorbent

UiO-66(NH_2) was synthesized according to Wang's method (Wang et al., 2017). In brief, 10.49 mg $ZrCl_4$, 8.15 mg H_2BDC-NH_2 and 1.2 mL acetic acid were mixed in 10 mL DMF solution to form a homogeneous solution by bath sonication. Afterwards, the mixture was sealed in a Teflon-lined autoclave and heated at 120 °C for 24 h in an oven. Before vacuum drying at 90 °C, the white products of UiO-66(NH_2) nanoparticles were collected by centrifuging (10,000 rpm, 5 min) and washed with methanol/DMF solution (v/v = 1:4) for three times. Highly dispersed Au nanoparticles were immobilized on UiO-66(NH_2) via reduction method described as follows: (1) 200 mg UiO-66(NH_2) was dispersed in 40 mL 0.025 M $HAuCl_4{\cdot}3H_2O$ solution containing water/methanol (1:1, v/v); (2) the mixture was continuously stirred in an ice bath for 1 h to accelerate the electrostatic interaction between NH_4^+ of UiO-66(NH_2) and $[AuCl_4]^-$; (3) $NaBH_4$ solution (10 mL, 0.05 M) was added and kept in an ice bath for 0.5 h to reduce the $[AuCl_4]^-$ into Au nanoparticle (Scheme 1); (4) the red products of UiO-66(NH_2)@Au were washed with methanol (10,000 rpm, 5 min) for three times. Finally, the UiO-66(NH_2)@Au was resuspended in 0.2 M Cys solution and stirred at room temperature for 24 h to obtain the UiO-66(NH_2)@Au-Cys nanocomposites (Ma et al., 2017).

2.3. Characterization

The morphologies of the obtained nanoparticles were characterized with S-4800 scanning electron microscopes (SEM, Hitachi, Tokyo, Japan). The X-ray diffraction (XRD) patterns of nanoparticles were obtained by a Bruker D8 Advanced Diffractometer System (Bruker AXS, Germany), which equipped with Cu Ka radiation source at an operating voltage of 40 kV. Fourier-transform infrared (FT-IR) spectra were collected by a Vetex70 (BRUKER Corp., Germany) equipped with a KBr beam splitter.

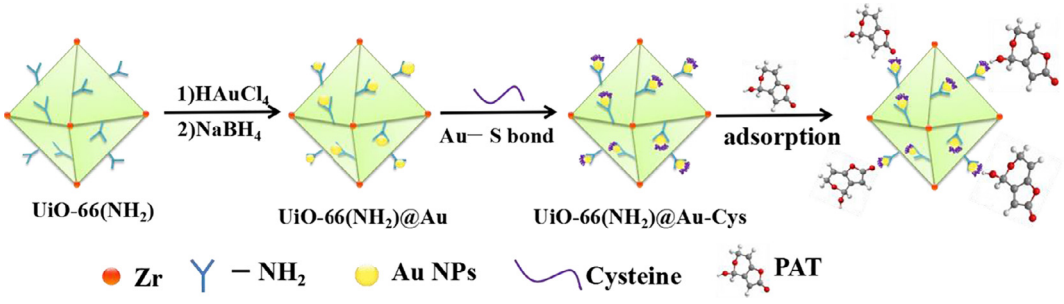

Scheme 1. Schematic representation of the UiO-66(NH_2)@Au-Cys and the PAT adsorption.

2.4. Batch adsorption experiments

2.4.1. Preparation of solutions

The adsorbent stock solution (3 g/L) was prepared by dissolving the dried adsorbent (UiO-66(NH_2)@Au-Cys) in fresh deionized water. The PAT stock solution in ethyl acetate (10 mg/L) was completely evaporated to dry by a gentle N_2 stream at 45 °C in a water bath, and then re-dissolved in acetic acid solution (pH 4.0) and stored in dark at 4 °C. The PAT working solutions with different concentrations ranging from 80 μg/L to 200 μg/L were prepared by diluting the stock solution with acetic acid solution (pH 4.0).

2.4.2. Effect of pH on PAT adsorption capacity by UiO-66(NH_2)@Au-Cys

To investigate the influence of pH on PAT adsorption capacity of UiO-66(NH_2)@Au-Cys, a series of PAT working solutions (200 μg/L) were mixed with adsorbent (0.3 g/L). The initial pH of PAT working solution was adjusted from 1 to 8 by adding negligible volume of 1 M acetic acid or 1 M NaOH. The PAT adsorption process was conducted at 35 °C for 3 h.

2.4.3. Adsorption kinetics

For kinetic studies, UiO-66(NH_2)@Au-Cys (0.3 g/L) was added into a flask containing 20 mL PAT working solution with a concentration of 200 μg/L. Subsequently, the pH was adjusted to 5.0 by adding negligible volume of 1 M NaOH, the mixture was kept at 35 °C. The PAT concentrations of the supernatant at different time interval were determined to elucidate the adsorption kinetics of the proposed adsorbents.

2.4.4. Adsorption isotherm

Adsorption isotherm experiments were performed at different temperature (25 °C, 35 °C and 45 °C) by adding 10 mg/L adsorbents into PAT working solutions with different concentrations ranged from 80 μg/L to 200 μg/L at pH 5.0 for 200 min. After adsorption, the adsorbents were separated by centrifugation (10,000 rpm, 5 min), the residual PAT in supernatant was determined by HPLC. The PAT adsorption capacity was calculated according to the equation (1). All of the experiments were repeated for three times.

$$q_t = (C_o - C_t)\frac{V}{W} \quad (1)$$

where q_t (μg/mg) was the adsorption capacity of per milligram adsorbent, C_0 (μg/L) was the initial concentraton of PAT, C_t (μg/L) was the concentration of residual PAT at adsorption time t, V was the volume of PAT aqueous solution (L) and W was the weight of the adsorbent (mg).

2.5. HPLC-UV analysis

A Shimadzu LC-15C system, equipped with degasser, quaternary pump, autosampler, WondaSil-C_{18} chromatographic column (4.6 × 250 mm; GL Science, Japan) and SPD-15C UV-detector (Shimadzu, Japan), was applied to detect PAT concentration. The mobile phase for isocratic elution was acetonitrile and water (1:9, v/v) with a flow-rate of 1 mL/min at column temperature of 30 °C. The injection volume was 20 μL, and the detection wavelength was 276 nm (Luo et al., 2017).

2.6. Apple juice quality analysis

The PAT-free apple juice (10.2 °Brix) sample was purchased from local retail markets and stored at 4 °C. For the propose of evaluating the availability of the adsorbent for practice application, the adsorption experiments was performed at 35 °C by adding 50 mg of adsorbent (calculated by equation (7)) into 30 mL PAT-contaminated (200 μg/L) apple juice. The quality parameters of apple juice including brix, titratable acidity, clarity, total phenol and vitamin C content were constantly measured at different adsorption time until reached equilibrium. According to the report (Luo, Li, Yuan, & Yue, 2016): (1) brix was measured by a hand refractometer (Atago, Tokyo, Japan); (2) titratable acidity was calculated by titrating with 0.1 mol/L NaOH; (3) clarity was measured by transmittance through a spectrophotometer (UV2550, Shimadzu Scientific Instruments) at 625 nm, using distilled water as a blank; (4) total phenol was evaluated by Folin-Ciocalteu method (Lee, Seo, Rhee, & Kim, 2016), using gallic acid as a reference compound; (5) Vitamin C was determined by 2,6-dichloroindophenol titration method described by GB 5009.86 (SAC, 2016). All of the determination experiments were conducted in triplicates.

2.7. Cytotoxicity evaluation

To evaluate the cytotoxicity of UiO-66(NH_2)@Au-Cys, NIH 3T3 cells (mouse fibroblast cells) were cultured for MTT assay according to Molavi's method (Molavi et al., 2018). It was reported that UiO-66(NH_2) was safe for human body (Molavi et al., 2018), thus which was selected as the positive control. The experiment was performed as follows. Firstly, 100 μL of NIH 3T3 cells were seeded in a 96-well plates at a density of 1×10^4 and incubated for attachment at 37 °C for 24 h. After removing 100 μL medium from each well, the cells were cultured in the medium with UiO-66(NH_2) and UiO-66(NH2)@Au-Cys at various concentrations ranging from 0 to 1000 μg/mL for 24 h. Subsequently, a final concentration of 0.5 mg/mL MTT was added and the mixture was incubated at 37 °C for 4 h. Before determination the absorbance at 570 nm, 100 μL DMSO was added and kept in room temperature for 10 min. The cells without being treated by UiO-66(NH_2) and UiO-66(NH2)@Au-Cys were taken as the control. Cell viability (%) was determined according to equation (2):

$$Cell\ viability\,(\%) = \frac{A_t}{A_c} \times 100\% \quad (2)$$

where A_t (a.u.) was the absorbance of UiO-66(NH_2) and UiO-66(NH_2)@Au-Cys treated cells, respectively. A_c (a.u.) was the absorbance of control.

2.8. Statistical analysis

IBM SPSS Statistics software 23.0 (IBM Corp., Armonk, NY, USA) was used to perform the statistical analysis, P value less than 0.05 was considered as statistically significant.

3. Results

3.1. Characterization of UiO-66(NH_2)@Au-Cys adsorbent

The morphologies of UiO-66(NH_2) and UiO-66(NH_2)@Au-Cys were characterized by SEM as shown in Fig. 1a and b, respectively. It was obvious that the octahedral shape of UiO-66(NH_2) did not change after loading Au nanoparticles. Due to the distribution of Au nanoparticles on the surface of UiO-66(NH_2), more distinct rough surface of UiO-66(NH_2)@Au-Cys compared with pure UiO-66(NH_2) could be observed. In order to characterize the chemical structure of UiO-66(NH_2) and further ascertain the presence of Cys moiety on the surface of UiO-66(NH_2)@Au-Cys, the FT-IR characterization was performed and the results were shown in Fig. 1c. There were several peaks derived from aromatic and carboxylic groups of 2-aminoterephthlic acid for the C–C vibrational mode (1420 cm^{-1}) and C–O bonding (1580 cm^{-1}) in the carboxylates (Kandiah et al., 2010). Two characteristic peaks of the primary amine were detected at 3515 and 3390 cm^{-1}, which was attributed to asymmetric and symmetric stretching modes of N–H bonding of the ligand, respectively. The bonding between aromatic carbon and nitrogen was also observed at 1260 and 1370 cm^{-1} (Kandiah et al., 2010). As shown in Fig. 1c (red line), the

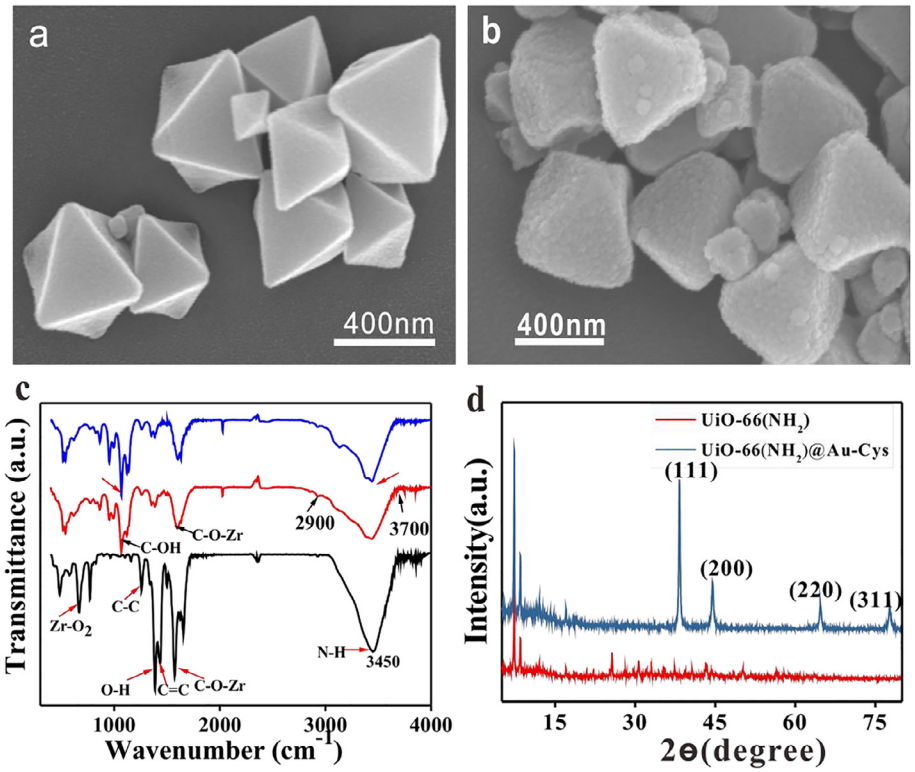

Fig. 1. SEM image for (a): UiO-66(NH_2); (b):Au loaded UiO-66(NH_2); (c): FTIR spectra for UiO-66(NH_2), pristine UiO-66(NH_2)@Au-Cys and UiO-66(NH_2)@Au-Cys after PAT adsorption, respectively; (d): XRD pattern of UiO-66(NH_2) and UiO-66(NH_2)@Au-Cys.

functionalization of cysteine was confirmed by the intensity increasing and position shifting of the peaks from 2900 cm^{-1} to 3700 cm^{-1}, which were attributed to vibrational modes of the –COOH group and N–H group. The successful immobilization of Au nanoparticles on UiO-66(NH_2) was further confirmed by powder X-ray diffraction (XRD) pattern. As shown in Fig. 1d, both UiO-66(NH_2) and UiO-66(NH_2)@Au-Cys displayed characteristic peaks of UiO-66(NH_2) at $2\theta \approx 7.2^{\circ}$ and 8.5°, which suggested that the immobilization of Au nanoparticles on UiO-66(NH_2) did not cause significant loss of the crystallinity. Moreover, UiO-66(NH_2)@Au-Cys showed the sharp characteristic peaks of Au at (1 1 1), (2 0 0), (2 2 0) and (3 1 1), which were well matched with the previous report (Luan, Qi, Gao, Zheng, & Wang, 2014; Peterson et al., 2016). XRD pattern of UiO-66(NH_2)@Au-Cys confirmed the immobilization of Au nanoparticles. This was congruent with SEM image, which also showed that the surface of UiO-66(NH_2)@Au-Cys was coarser than the bare UiO-66(NH_2). The above results demonstrated that the novel adsorbent was successfully prepared, thus Cys could provide abundant active groups for PAT adsorption.

3.2. Batch adsorption analysis

3.2.1. Effect of pH on PAT adsorption by UiO-66(NH_2)@Au-Cys

The acidity of the sample solution affected the surface chemical properties of UiO-66(NH_2)@Au-Cys and the physicochemical properties of PAT. Thus, the effect of pH on the adsorption capacity of the adsorbent was investigated. As shown in Fig. 2a, the adsorption capacity significantly increased from 19 to 24 μg/mg at pH 5.0 to 8.0, while did not fluctuate obviously at pH 1.0 to 4.0 ($P > 0.05$). It was caused by the protonation of hydroxyl and amino groups accelerated the competition between protonated H^+ and PAT at low pH solution (Peng et al., 2016; Wang et al., 2016), which leaded to a low adsorption capacity. Particularly, there was no obvious decreasing of adsorption capacity for UiO-66(NH_2)@Au-Cys at strong acid condition (pH = 1), which indicated that the prepared adsorbent has a good stability against acidic juice. As the apple juice was slightly acidic and PAT was unstable at pH > 6.0 (Valle-Algarra, Mateo, Gimeno-Adelantado, Mateo-Castro, & Jiménez, 2009), the adsorption kinetics and isotherms were performed at pH 5.0.

3.2.2. Effect of adsorption time on PAT adsorption by UiO-66(NH_2)@Au-Cys

As the adsorption time was an important to adsorption. PAT adsorption capacity of UiO-66(NH_2)@Au-Cys at different adsorption time was investigated. As shown in Fig. 2b, PAT adsorption capacity of UiO-66(NH_2)@Au-Cys rapidly increased when increasing adsorption time ($P < 0.05$), which suggested that the adsorption process was not in a constant speed (Luo et al., 2016). Moreover, there was no obvious increasing of the PAT adsorption capacity of UiO-66(NH_2)@Au-Cys beyond 3 h ($P > 0.05$), which indicated that 3 h was enough to reach the adsorption equilibrium. Thus, 3 h was chosen as the adsorption time for the following experiments. Comparing with microbial adsorbents (like yeast and lactic acid bacteria), the adsorption time of UiO-66(NH_2)@Au-Cys was shortened significantly from 20 or 24 h to 3 h (Qiu et al., 2018; Wang et al., 2015), which was ascribed to the acceleration of PAT removal caused by the abundant adsorption sites on the surface of the proposed adsorbent.

3.2.3. Adsorption kinetics

As a fundamental method for studying adsorption mechanism, adsorption kinetics was performed in this study. The Pseudo-first-order kinetics model (3) and Pseudo-second-order kinetics model (4) were applied to investigate the adsorption kinetics according to the following equations, and the fitting curves were show in Fig. 2c and d.

$$\log(q_e - q_t) = \log q_e - \frac{k_1 t}{2.303} \quad (3)$$

$$\frac{t}{q} = \frac{1}{k_2 q_e^2} + \frac{t}{q_t} \quad (4)$$

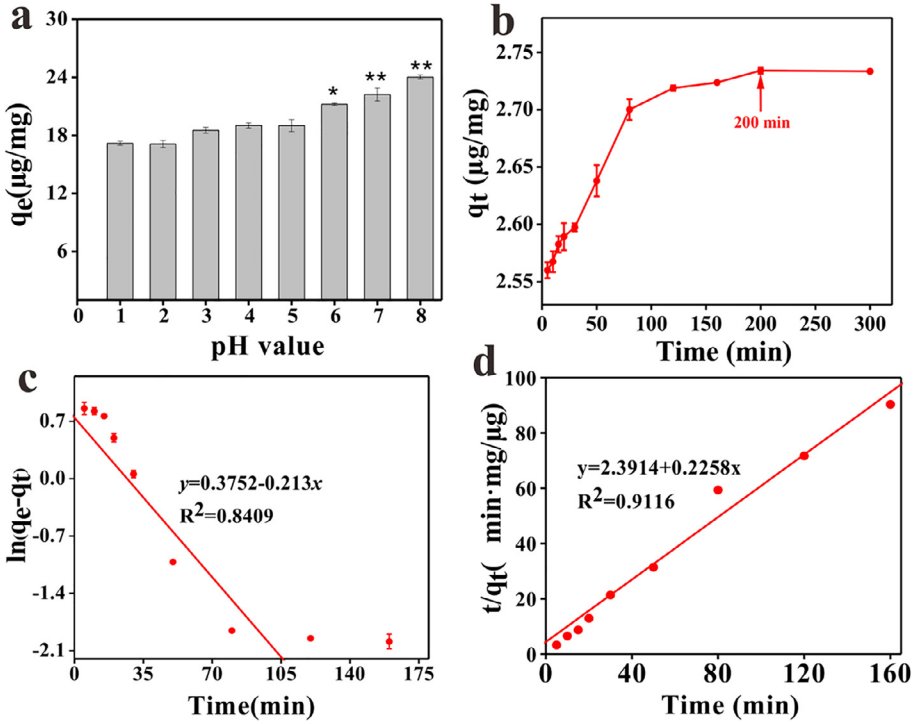

Fig. 2. (a): Effect of pH values on adsorption of PAT, bars marked with (*) are significantly different, $^{*}P < 0.05$, $^{**}P < 0.01$; (b): Time profile for PAT adsorption; (c) and (d): Plots of Pseudo-first and Pseudo-second order kinetic models for PAT adsorption on the adsorbent, respectively.

where q_e (μg/mg) and q_t (μg/mg) were the amounts of PAT adsorbed onto the nanosorbent at equilibrium and time t (min), respectively. k_1 (min^{-1}) and k_2 ($mg{\cdot}\mu g^{-1}{\cdot}min^{-1}$) were the rate constant of Pseudo-first-order and Pseudo-second-order kinetic model, respectively.

The obtained kinetic parameters were present in Table S1. According to the correlation coefficient values ($R^2 = 0.9116$) obtained from the linear regression analysis, the results were obviously fitted by Pseudo-second-order kinetic model, which suggested that the chemisorption (*i.e.*, covalent) between PAT and the binding sites on the adsorbent was the rate-limiting step of adsorption (Anene, Kalfat, Chevalier, & Hbaieb, 2016). Additionally, according to pseudo-second-order model, the calculated equilibrium adsorption amount ($q_e = 4.43$ μg/mg) of PAT on UiO-66(NH_2)@Au-Cys was approximately to the value measured in the experiments (4.18 ± 0.063 μg/mg). Moreover, the amount of equilibrium adsorption capacity of PAT was 10 times higher than the inactivated yeast and lactic acid bacteria, which were summarized in Table 1. It was reported that the complex pretreatment of inactivated microorganism resulted in the inevitable destruction in cell wall, which was the main reason for the decreasing of the adsorption capacity (Li, 2014; Liu et al., 2015; Luo et al., 2015; Wang et al., 2015). Compared with the microbe-based adsorbents, UiO-66(NH_2)@Au-Cys was more chemical stable and with high adsorption capacity for PAT, which indicated that UiO-66(NH_2)@Au-Cys was promising to satisfy the practical industrial requirement for PAT removal. Furthermore, the Pseudo-second-order model demonstrated that the chemisorption was the rate limiting step of adsorption. To further investigate the function sites of PAT adsorption, the FT-IR spectrum of UiO-66(NH_2)@Au-Cys after PAT adsorption was characterized. As presented in Fig. 1c, the spectra of the pristine UiO-66(NH_2)@Au-Cys (marked by red line) and PAT-adsorbed UiO-66(NH_2)@Au-Cys (marked by blue line) were almost consistent, but the intensity band at around 3450 cm^{-1} of PAT-adsorbed UiO-66(NH_2)@Au-Cys increased compared with pristine UiO-66(NH_2)@Au-Cys. This indicated that the –NH_2 and –OH groups of UiO-66(NH_2)@Au-Cys played an important role in the reaction with the hydroxy and carbonyl groups of PAT (chemical structure was shown in Fig. S1). It was in agreement with the previous findings that demonstrated the adsorption of biosorbents for PAT was mainly attributed to the large amount of functional groups of proteins and carbohydrates in cell wall, such as C–O, O–H and N–H (Hatab, Yue, & Mohamad, 2012).

Although pseudo-second-order model was well fitted with the experimental data, the obtained information was not sufficient to illustrate the diffusion mechanism. The adsorption for the target on the solid surface involved several successive steps: (1) the transportation of the

Table 1
Comparasion of parameters for PAT adsorption on different adsorbents.

Adsorbents	Adsorption capacity (μg/mg)	Adsorption time (h)	Reference
Inactivated yeast	0.012	30	Luo et al., 2016
Inactivated LAB	0.52	48	Wang et al., 2015
Fe_3O_4-chitosan-yeast	0.0095	15	Ge, Xu, Li, Peng, & Pan, 2017
Fe_3O_4@chitosan NPs	6.67	5	Luo et al., 2017
Thiorea modified chitosan	1	24	Liu et al., 2015
Cross-linked xanthated chitosan	23.81	18	Peng et al., 2016
Cross-linked chitosan	0.63	24	Li et al., 2015
SBA-15-PSH	6.27	8	Appell et al., 2011
Ca-alginate-Actived carbon	0.0034	5	Yue et al., 2013
UiO-66(NH_2)@Au-Cys	4.18	< 3.5	This work

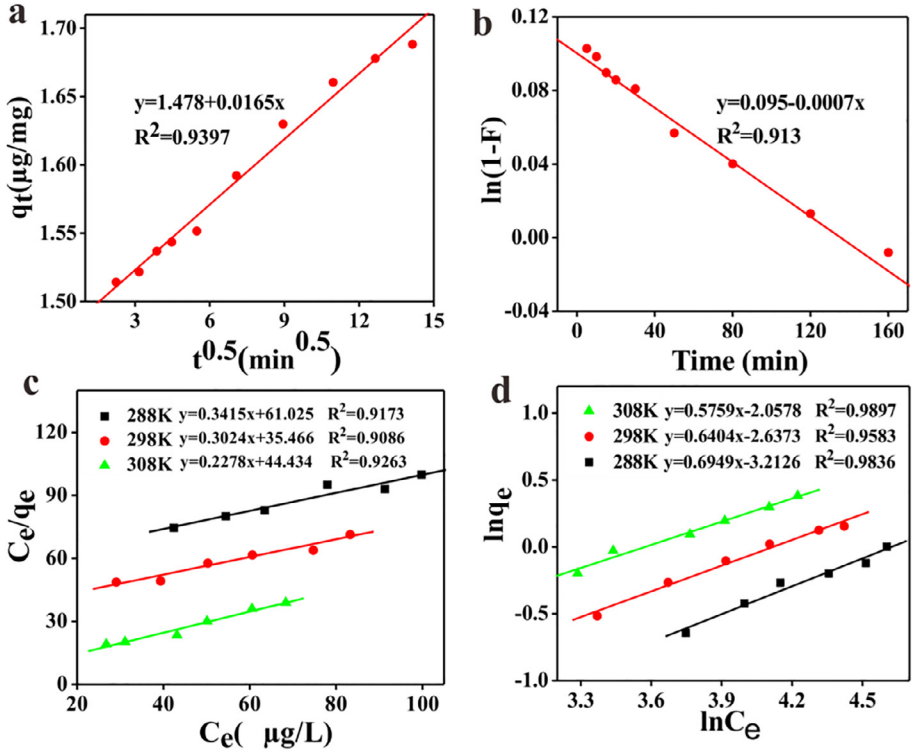

Fig. 3. (a): Plots for liquid film diffusion model; (b): Plots for intraparticle diffusion model; (c): Langmuir adsorption isotherm curves; (d): Freundlich adsorption isotherm curves.

adsorbate molecule from bulk solution to the adsorbent surface through a quiescent liquid film (boundary layer diffusion); (2) the diffusion into the pores of the material (intraparticle diffusion); (3) the adsorption at the surface of the adsorbent. As the last step accomplished fast, so that the adsorption process was always rate-controlled by the first two steps (Wang et al., 2016). To identify the rate-controlled step for PAT adsorption process under the experimental conditions, the liquid film diffusion models (5), (6) as well as intraparticle diffusion model (7) were conducted to fit the experimental data according to the following equation. The fitting lines are showed in Fig. 3a and b.

$$\ln(1-F) = C - k_{fd}t \tag{5}$$

$$F = \frac{q_t}{q_e} \tag{6}$$

$$q_t = k_{fd}t^{0.5} + C \tag{7}$$

where q_e and q_t (μg/mg) were the amounts of PAT adsorbed onto adsorbent at equilibrium and any time t (min), respectively. k_{fd} was the liquid film diffusion constant (min^{-1}), k_{id} was the intraparticle diffusion rate constant ($\mu g/mg \cdot min^{0.5}$).

The liquid film diffusion model and intraparticle diffusion model were summarized in Table S2. According to the comparison of the correlation coefficient between the two diffusion models, intraparticle diffusion model was better for describing the diffusion mechanisms. The plot of intraparticle diffusion model didn't pass through the zero point, which demonstrated that the intraparticle diffusion was not the only rate-limiting step for adsorption (Wang et al., 2016). In addition, the plot of the liquid film diffusion model displayed linear profiles (Fig. 3b), which partly explained that the rate controlling step was mass transfering in liquid film (Liu et al., 2015; Qiu et al., 2018).

3.2.4. Adsorption isotherms

Adsorption isotherms were used to reveal the relationship between the equilibrium concentration (C_e) of the system and the amount of adsorbed PAT (q_e). Two classical isotherm models including Langmuir (8) and Freundlich (9) models were introduced to examine the experimental data, respectively. The corresponding equations were displayed as follows:

$$\frac{C_e}{q_e} = \frac{1}{q_s k_b} + \frac{C_e}{q_s} \tag{8}$$

$$\ln q_e = \ln k_F + \frac{1}{n}\ln C_e \tag{9}$$

where q_e was the adsorption capacity of the adsorbent at equilibrium (μg/mg), C_e was the concentration of PAT in the equilibrium solution (μg/L) and q_s (μg/mg) was the theroretical maximum adsorption capacity. The parameter k_b was the Langmuir adsorption equilibrium constant (L/μg). Moreover, k_F ($\mu g^{1-n} L^n mg^{-1}$) and n were the constants of the Freundlich isotherm equation. The constants including q_s, k_b, k_F and n were deduced from the slope and intercept of the corresponding linear plot.

All of the fitting lines were shown in Fig. 3c and d. The fitting parameters of Langmuir and Freundlich models were given in Table S3. As shown in Fig. 3c and d, the adsorption capacities increased with the raise of initial PAT concentration as the higher initial concentration provided more driving force to enhance the effective contact between PAT with the adsorbent (Qiu et al., 2018). The maximum adsorption capacity calculated from the Langmuir isotherm model was 4.38 μg/mg, which was similar to the q_e calculated by Pseudo-second-order model. Obviously, the adsorption capacity of UiO-66(NH_2)@Au-Cys was 10 times higher than the microbe-based biosorbents and cross-linked chitosan, which was shown in Table 1. Accordingly, UiO-66(NH_2)@Au-Cys was a promising adsorbent for PAT removal in future application. Besides, the comparison of the R^2 values between Langmuir isotherm model and Freundlich isotherm model suggested that Freundlich isotherm model performed a better fit to the experimental data than Langmuir isotherm model, which revealed that the PAT adsorption was based on multi-layer adsorption. Freundlich isotherm depicts non-ideal adsorption that there has a heterogeneous distribution of active sites in the adsorbent surfaces, thus generating a multilayer adsorption

between the adsorbent and adsorbate. Furthermore, in Freundlich isotherm model, 1/n was a significant parameter to evaluate the degree of the preferential adsorption (Qiu et al., 2018): unfavorable (1/n > 1), favorable (0 < 1/n < 1) and irreversible (1/n = 1). In our case, the adsorption of PAT was favorable according to the value of 1/n in Table S3.

3.2.5. Thermodynamic analysis

To investigate the effect of the temperature on the PAT adsorption, the adsorption process was studied at 288 K, 298 K and 308 K, respectively. The thermodynamic parameters including standard Gibbs free energy change (ΔG^o), standard enthalpy change (ΔH^o) and standard entropy change (ΔS^o) were determined according to equation (10):

$$K_c = \frac{q_e}{C_e}$$

$$\Delta G^o = -R \ln K_c$$

$$\ln K_c = \frac{\Delta S^o}{R} - \frac{\Delta H^o}{RT} \quad (10)$$

The q_e and C_e were the adsorption capacity and equilibrium concentration of PAT, respectively. T (K) was the temperature during adsorption, R (8.3145 J·mol^{-1}·K^{-1}) was the ideal gas constant, K_c was the thermodynamic equilibrium constant. ΔH^o and ΔS^o were calculated by the slope and intercept obtained by lnK_c-1/T fitting.

The thermodynamic parameters were shown in Table S4. The overall ΔG^o was negative and decreased with the increase of temperature, which indicated that the adsorption process was spontaneous and favorable at higher temperatures. The positive ΔH^o confirms that the adsorption process was endothermic, which also suggested that the nature of chemisorption. The positive value of ΔS^o showed an increased randomness at solid-solution interface (Qiu et al., 2018). In addition, the solution viscosity decreased at the higher temperature, which resulted in the increasing of PAT mobility and enhanced the interaction of PAT with the active sites in UiO-66(NH_2)@Au-Cys (Yu et al., 2011).

3.3. Effect of UiO-66(NH_2)@Au-Cys on PAT adsorption in apple juice

To evaluate the feasibility of UiO-66(NH_2)@Au-Cys in practical application, the adsorption capacity and variations of juice quality index (brix, titratable acidity, clarity, total phenol and vitamin C content) were measured during PAT removal from apple juice. As shown in Fig. 4a, the PAT adsorption capacity of UiO-66(NH_2)@Au-Cys increased with the adsorption time and reached equilibrium at 70 min. After adsorption, 87% of the total PAT were removed, which resulted in the concentration of PAT in apple juice was below the standard concentration recommended by WHO (50 μg/kg). The adsorption time was shortened considerably compared with other adsorbents such as inactivated yeast, lactic acid bacteria and chitosan-based sorbents that listed in Table 1. Moreover, as shown in Table S5, the final PAT removal rate UiO-66(NH_2)@Au-Cys in acetic solution was higher than that in apple juice ($P < 0.05$), while the PAT removal rate in acetic solution was lower than in apple juice for the first 80 min ($P < 0.05$). A suitable reason to explain the observed decrease of adsorption capacity was that the lone pair electrons of –NH_2 and –OH groups presented on UiO-66(NH_2)@Au-Cys could bond with some metal ions and compounds like organic acid in apple juice (Peng et al., 2016). In contrast, the complex composition of juice and the interference effect of some small molecules might bond with the active sites of the adsorbent to reach equilibrium (Luo et al., 2016). Thus, the time required to achieve the adsorption equilibrium was 70 min, which was shortened by one third compared to the adsorption time in acetic acid aqueous. Additionally, during PAT adsorption process, the changes in brix, titratable acidity, clarity, total phenol and vitamin C content of apple juice were obtained as shown in Fig. 4b-f, respectively. No significant changes in brix, clarity and total phenol content were observed ($P > 0.05$). A slightly decrease was observed in titratable acidity (from 7.19 ± 0.043 to 6.86 ± 0.011 g/L) and vitamin C content (from 174.42 ± 0.013 to 174.39 ± 0.012 mg/L) ($P < 0.05$). The results also revealed that PAT bonding was not extremely specific, for example, the organic acids in apple juice could provide more protons that would be available to bond with amine groups of the adsorbent, which was also the main reason for the slight and accetable reduction of titratable acidity and vitamin C content. Therefore, UiO-66(NH_2)@Au-Cys was a potential adsorbent that could be applied to the apple juice industry for PAT removal.

3.4. Cytotoxicity of UiO-66(NH_2) and UiO-66(NH_2)@Au-Cys

NIH 3T3 cell lines were frequently used to investigate the biocompatibility of nanoparticles (Molavi et al., 2018). The cytotoxicity of UiO-66(NH_2)@Au-Cys against the NIH 3T3 cell line was studied by MTT assays. Fig. 5 showed the viability of the cultured cells in the

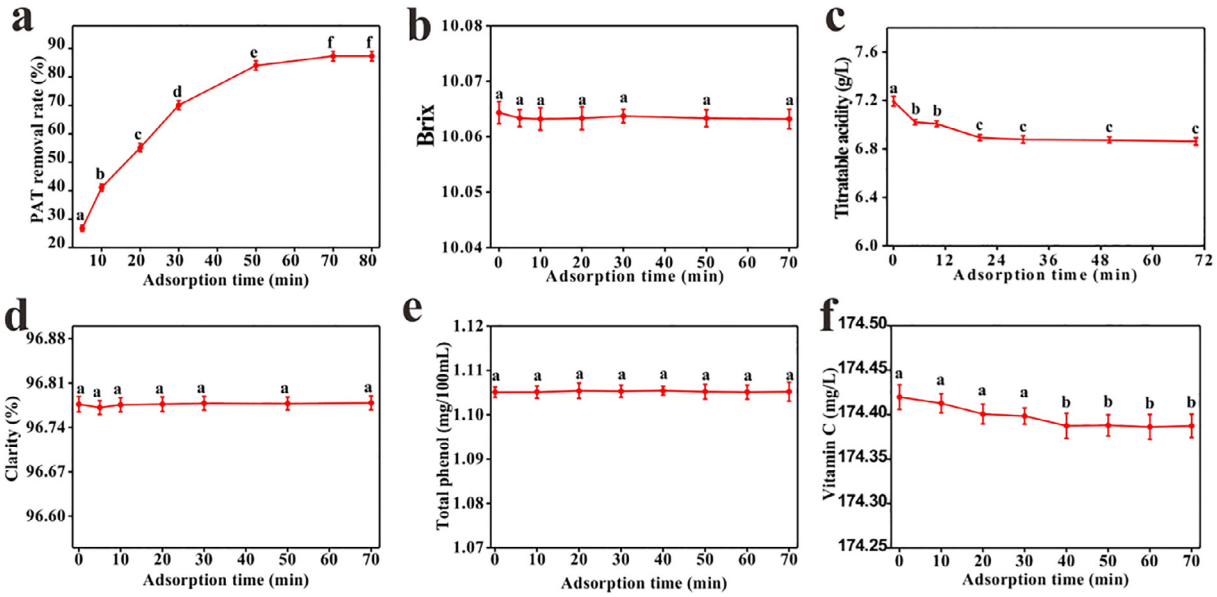

Fig. 4. Changes in (a): PAT removal rate; (b): brix; (c): titratable acidity; (d): clarity; (e): total phenol and (f): vitamin C content during the process of PAT adsorption from apple juice. Values are the means ± SD, different lowercase letters in a curve represents significant difference ($P < 0.05$).

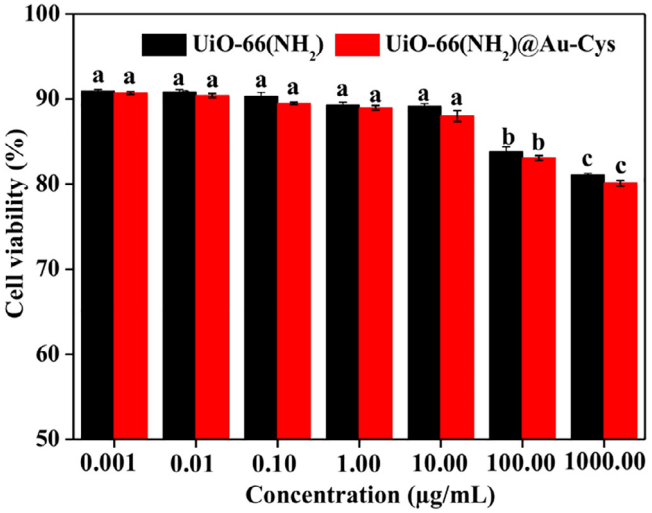

Fig. 5. Viability of NIH 3 T3 cells treated with different concentrations of UiO-66(NH_2) and UiO-66(NH_2)@Au-Cys, same color bars marked with different lowercase letters represented significant difference($P < 0.05$).

presence of UiO-66(NH_2) and UiO-66(NH_2)@Au-Cys at the concentrations range of 0.001–1000 μg/mL. The cell viability presented a gradual decrement trend with the increasing UiO-66(NH_2) and UiO-66(NH_2)@Au-Cys concentration. A significant ($P < 0.05$) reduction in cell viability was observed at 100 μg/mL and 1000 μg/mL for UiO-66(NH_2) and UiO-66(NH_2)@Au-Cys, respectively. There was no significant difference in cell viability between UiO-66(NH_2) treated cells and UiO-66(NH_2)@Au-Cys treated cells, and the cell viability still higher than 80% even the treated does of UiO-66(NH_2) and UiO-66(NH_2)@Au-Cys as high as 1000 μg/mL. Moreover, no significant decrease in cell viability was observed when the concentration of both UiO-66(NH_2) and UiO-66(NH_2)@Au-Cys was less than 10 μg/mL ($P < 0.05$), where the cell viability was over 90%. Importantly, the residual concentration of the adsorbent in apple juice was 0.12 ± 0.0036 μg/mL, which was too low to cause cytotoxicity. However, there still need a systematic study about the safety of the proposed adsorbent. Therefore, the potential use of UiO-66(NH_2)@Au-Cys as PAT adsorbent in apple juice should be further elucidated.

4. Conclusion

In summary, nontoxic zirconium-based absorbent (UiO-66(NH_2)@Au-Cys) was successfully synthesized and used for removal of PAT from apple juice. The kinetic and isotherm study revealed that PAT adsorption process was well described by Pseudo-second order model and Freundlich model, respectively. The maximum adsorption capacity was of 4.38 μg/mg, which was 10 times higher than inactivated microorganisms, and the adsorption time was significantly shortened from 24 h to 3 h. Thermodynamic studies confirmed that the adsorption was an endothermic and spontaneous process. FI-IR spectra illustrated that amine, hydroxyl and carboxyl were mainly responsible for PAT binding. Moreover, the residual UiO-66(NH_2)@Au-Cys in apple juice did not cause marked cytotoxicity for NIH 3 T3 cells. Therefore, this novel MOF-based adsorbent was a potential adsorbent to be applied for PAT removal in the apple juice industry

Acknowledgement

This research was financed by Grants from National Natural Science Foundation of China (No. 21675127), the Development Project of Qinghai Key Laboratory (No. 2017-ZJ-Y10) and Fundamental Research Funds for the Northwest A&F University of China (2014YB093, 2452015257).

Appendix A. Supplementary data

Supplementary data associated with this article can be found, in the online version, at https://doi.org/10.1016/j.foodchem.2018.07.072.

References

Anene, A., Kalfat, R., Chevalier, Y., & Hbaieb, S. (2016). Molecularly imprinted polymer-based materials as thin films on silica supports for efficient adsorption of Patulin. *Colloids and Surfaces A: Physicochemical and Engineering Aspects, 497*, 293–303.

Appell, M., & Jackson, M. A. (2010). Synthesis and evaluation of cyclodextrin-based polymers for patulin extraction from aqueous solutions. *Journal of Inclusion Phenomena and Macrocyclic Chemistry, 68*(1–2), 117–122.

Appell, M., Jackson, M. A., & Dombrink-Kurtzman, M. A. (2011). Removal of patulin from aqueous solutions by propylthiol functionalized SBA-15. *Journal of Hazardous Materials, 187*(1), 150–156.

Beltrán, E., Ibáñez, M., Sancho, J. V., & Hernández, F. (2014). Determination of patulin in apple and derived products by UHPLC–MS/MS. Study of matrix effects with atmospheric pressure ionisation sources. *Food Chemistry, 142*, 400–407.

Boussabbeh, M., Ben Salem, I., Neffati, F., Najjar, M. F., Bacha, H., & Abid-Essefi, S. (2015). Crocin prevents patulin-induced acute toxicity in cardiac tissues via the regulation of oxidative damage and apoptosis. *Journal of Biochemical and Molecular Toxicology, 29*(10), 479–488.

Cavka, J. H., Jakobsen, S., Olsbye, U., Guillou, N., Lamberti, C., Bordiga, S., et al. (2008). A new zirconium inorganic building brick forming metal organic frameworks with exceptional stability. *Journal of the American Chemical Society, 130*(42), 13850–13851.

Ge, N., Xu, J., Li, F., Peng, B., & Pan, S. (2017). Immobilization of inactivated microbial cells on magnetic Fe_3O_4@CTS nanoparticles for constructing a new biosorbent for removal of patulin in fruit juice. *Food Control, 82*, 83–90.

Hatab, S., Yue, T., & Mohamad, O. (2012). Removal of patulin from apple juice using inactivated lactic acid bacteria. *Journal of Applied Microbiology, 112*(5), 892–899.

Kandiah, M., Usseglio, S., Svelle, S., Olsbye, U., Lillerud, K. P., & Tilset, M. (2010). Post-synthetic modification of the metal-organic framework compound UiO-66. *Journal of Materials Chemistry, 20*(44), 9848–9851.

Lee, B., Seo, J. D., Rhee, J.-K., & Kim, C. Y. (2016). Heated apple juice supplemented with onion has greatly improved nutritional quality and browning index. *Food Chemistry, 201*, 315–319.

Li, Z. (2014). Synthesis of a carbamide-based dithiocarbamate chelator for the removal of heavy metal ions from aqueous solutions. *Journal of Industrial and Engineering Chemistry, 20*(2), 586–590.

Li, Y., Wang, J., Meng, X., & Liu, B. (2015). Removal of patulin from aqueous solution using cross-linked chitosan beads. *Journal of Food Safety, 35*(2), 248–256.

Liu, B., Peng, X., Chen, W., Li, Y., Meng, X., Wang, D., et al. (2015). Adsorptive removal of patulin from aqueous solution using thiourea modified chitosan resin. *International Journal of Biological Macromolecules, 80*, 520–528.

Luan, Y., Qi, Y., Gao, H., Zheng, N., & Wang, G. (2014). Synthesis of an amino-functionalized metal-organic framework at a nanoscale level for gold nanoparticle deposition and catalysis. *Journal of Materials Chemistry A, 2*(48), 20588–20596.

Luo, Y., Li, Z., Yuan, Y., & Yue, T. (2016). Bioadsorption of patulin from kiwi fruit juice onto a superior magnetic chitosan. *Journal of Alloys and Compounds, 667*, 101–108.

Luo, Y., Wang, J., Liu, B., Wang, Z., Yuan, Y., & Yue, T. (2015). Effect of yeast cell morphology, cell wall physical structure and chemical composition on patulin adsorption. *PLOS ONE, 10*(8), e0136045.

Luo, Y., Wang, Z., Yuan, Y., Zhou, Z., & Yue, T. (2016). Patulin adsorption of a superior microorganism strain with low flavour-affection of kiwi fruit juice. *World Mycotoxin Journal, 9*(2), 195–203.

Luo, Y., Zhou, Z., & Yue, T. (2017). Synthesis and characterization of nontoxic chitosan-coated Fe_3O_4 particles for patulin adsorption in a juice-pH simulation aqueous. *Food Chemistry, 221*, 317–323.

Ma, W., Xu, L., Li, X., Shen, S., Wu, M., Bai, Y., et al. (2017). Cysteine-functionalized metal-organic framework: Facile synthesis and high efficient enrichment of N-linked glycopeptides in cell lysate. *ACS Applied Materials & Interfaces*.

Moake, M. M., Padilla-Zakour, O. I., & Worobo, R. W. (2005). Comprehensive review of patulin control methods in foods. *Comprehensive Reviews in Food Science and Food Safety, 4*(1), 8–21.

Molavi, H., Zamani, M., Aghajanzadeh, M., Manjili, H. K., Danafar, H., & Shojaei, A. (2018). Evaluation of UiO-66 metal organic framework as an effective sorbent for Curcumin's overdose. *Applied Organometallic Chemistry, 32*(4).

Peng, X., Liu, B., Chen, W., Li, X., Wang, Q., Meng, X., et al. (2016). Effective biosorption of patulin from apple juice by cross-linked xanthated chitosan resin. *Food Control, 63*, 140–146.

Peterson, G. W., Mahle, J. J., DeCoste, J. B., Gordon, W. O., & Rossin, J. A. (2016). Extraordinary NO_2 removal by the metal-organic framework UiO-66-NH_2. *Angewandte Chemie International Edition, 55*(21), 6235–6238.

Puel, O., Galtier, P., & Oswald, I. P. (2010). Biosynthesis and toxicological effects of patulin. *Toxins, 2*(4), 613–631.

Qiu, Y., Guo, H., Guo, C., Zheng, J., Yue, T., & Yuan, Y. (2018). One-step preparation of nano-Fe_3O_4 modified inactivated yeast for the adsorption of patulin. *Food Control, 86*, 310–318.

SAC. GB 5009.86 (2016). *National food safety standard. Determination of ascorbic acid in food.* Beijing: China Standards Press.

Sanzani, S., Reverberi, M., Punelli, M., Ippolito, A., & Fanelli, C. (2012). Study on the role of patulin on pathogenicity and virulence of Penicillium expansum. *International*

Journal of Food Microbiology, 153(3), 323–331.
Tannous, J., Keller, N. P., Atoui, A., El Khoury, A., Lteif, R., Oswald, I. P., et al. (2017). Secondary metabolism in Penicillium expansum: Emphasis on recent advances in patulin research. *Critical Reviews in Food Science and Nutrition,* 1–17.
US Food and Drug Administration. (2013). CPG Sec. 510.150. Apple juice, apple juice concentrates, and apple juice products—adulteration with patulin. https://www.fda.gov/iceci/compliancemanuals/compliancepolicyguidancemanual/ucm074427.htm.
Valle-Algarra, F. M., Mateo, E. M., Gimeno-Adelantado, J. V., Mateo-Castro, R., & Jiménez, M. (2009). Optimization of clean-up procedure for patulin determination in apple juice and apple purees by liquid chromatography. *Talanta, 80*(2), 636–642.
Wang, X., Chen, W., Zhang, L., Yao, T., Liu, W., Lin, Y., et al. (2017). Uncoordinated amine groups of metal-organic frameworks to anchor single Ru sites as chemoselective catalysts toward the hydrogenation of quinoline. *Journal of the American Chemical Society, 139*(28), 9419–9422.
Wang, L., Wang, Z., Yuan, Y., Cai, R., Niu, C., & Yue, T. L. (2015). Identification of key factors involved in the biosorption of patulin by inactivated lactic acid bacteria (LAB) cells. *PLOS ONE, 10*(11), e0143431.
Wang, J., Zhang, W., Yue, X., Yang, Q., Liu, F., Wang, Y., et al. (2016). One-pot synthesis of multifunctional magnetic ferrite-MoS_2-carbon dot nanohybrid adsorbent for efficient Pb (ii) removal. *Journal of Materials Chemistry A, 4*(10), 3893–3900.
Yang, Q., Wang, J., Chen, X., Yang, W., Pei, H., Hu, N., et al. (2018a). The simultaneous detection and removal of organophosphorus pesticides by a novel Zr-MOF based smart adsorbent. *Journal of Materials Chemistry A*.
Yang, Q., Wang, Y., Wang, J., Liu, F., Hu, N., Pei, H. N., et al. (2018). High effective adsorption/removal of illegal food dyes from contaminated aqueous solution by Zr-MOFs (UiO-67). *Food Chemistry, 254*, 241–248.
Yu, X. Y., Luo, T., Zhang, Y. X., Jia, Y., Zhu, B. J., Fu, X. C., et al. (2011). Adsorption of lead (II) on O_2-plasma-oxidized multiwalled carbon nanotubes: Thermodynamics, kinetics, and desorption. *ACS Applied Materials & Interfaces, 3*(7), 2585–2593.
Yue, T., Guo, C., Yuan, Y., Wang, Z., Luo, Y., & Wang, L. (2013). Adsorptive removal of patulin from apple juice using Ca-alginate-activated carbon beads. *Journal of Food Science, 78*(10), 1629–1635.
Yun, H., Lim, S., Jo, C., Chung, J., Kim, S., Kwon, J.-H., et al. (2008). Effects of organic acids, amino acids and ethanol on the radio-degradation of patulin in an aqueous model system. *Radiation Physics and Chemistry, 77*(6), 830–834.